

## **Isolation of a chiral anthracene cation radical: X-ray crystallography and computational interrogation of its racemization**

Maxim V. Ivanov, Khushabu Thakur, Anshul Bhatnagar, and Rajendra Rathore\*

*Department of Chemistry, Marquette University, P.O. Box 1881, Milwaukee, WI 53201-1881*

### **Supporting Information**

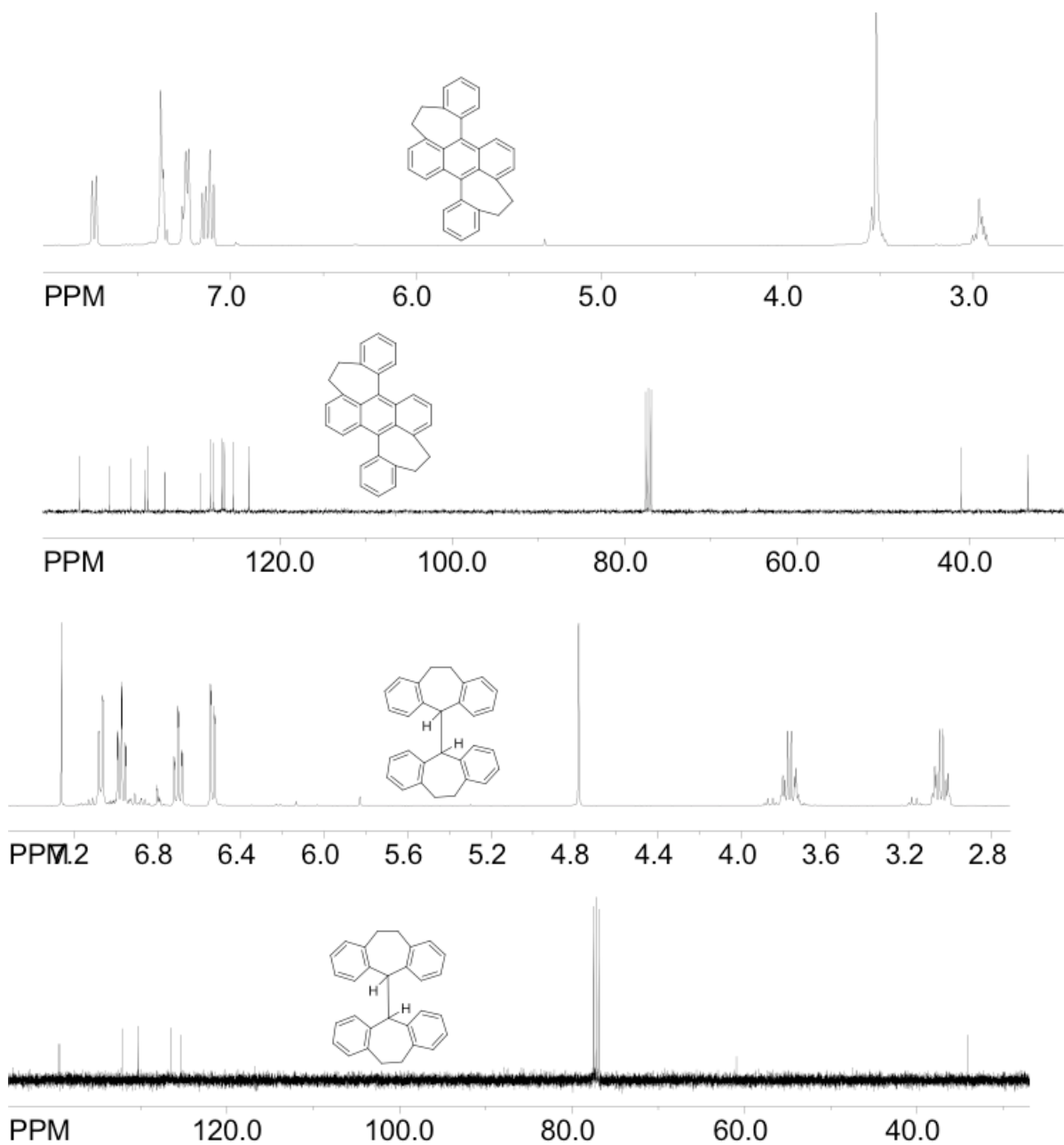
#### Table of Content

<b>S1. SYNTHESIS</b>	<b>2</b>
<b>S2. GENERATION OF CATION RADICALS</b>	<b>3</b>
<b>S3. X-RAY CRYSTALLOGRAPHY</b>	<b>5</b>
<b>S4. DENSITY FUNCTIONAL THEORY CALCULATIONS</b>	<b>6</b>
Computational Details	6
Isomerization Pathways	7
<b>S5. KINETIC MODELING</b>	<b>14</b>
<b>S6. REFERENCES</b>	<b>18</b>

## S1. Synthesis

A chiral 9,10-diphenyleanthracene derivative (i.e.  $S$ ANT) was synthesized following closely the literature procedures.<sup>1,2</sup> Chromatography of the crude reaction mixture afforded  $S$ ANT as the major product and tetrahydro-5,5'-bis(dibenzodicycloheptenyl) as a minor product.

### $^1H$ and $^{13}C$ NMR spectra of $S$ ANT



### UV-vis absorption spectroscopy

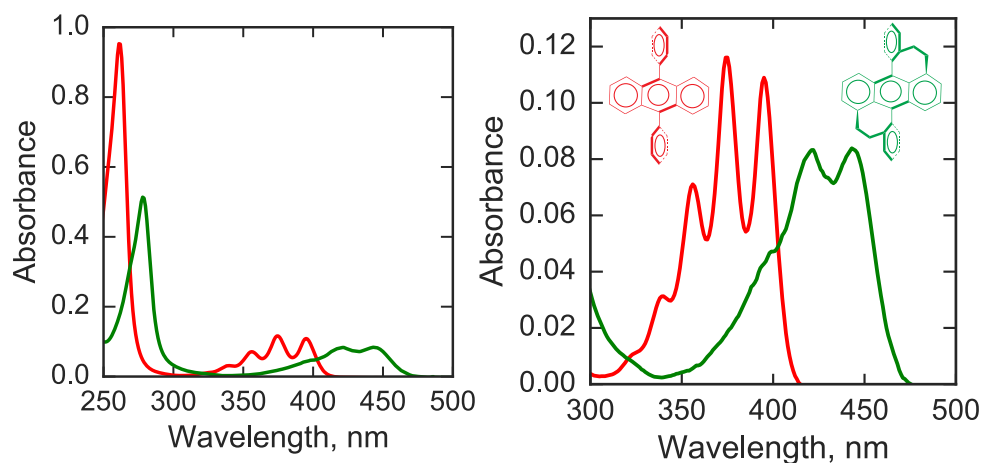


**Figure S1.** UV-vis absorption spectra of 9,10-diphenyl anthracene and doubly bridged 9,10-diphenyl anthracene in the range of 250-500 nm (left) and expanded to 300-500 nm range (right).

## S2. Generation of Cation Radicals

Reproducible spectra of doubly bridged 9,10-diphenyl anthracene (<sup>s</sup>ANT) and 9,10-diphenyl anthracene cation radicals were obtained in CH<sub>2</sub>Cl<sub>2</sub> solution at 22 °C by quantitative redox titrations using **THEO**<sup>+</sup>SbCl<sub>6</sub><sup>-</sup> ( $E_{\text{red1}} = 0.67$  V vs Fc/Fc<sup>+</sup>,  $\lambda_{\text{max}} = 518$  nm,  $\epsilon_{\text{max}} = 7300$  cm<sup>-1</sup> M<sup>-1</sup>),<sup>3</sup> and **NAP**<sup>+</sup>SbCl<sub>6</sub><sup>-</sup> ( $E_{\text{red1}} = 0.94$  V vs Fc/Fc<sup>+</sup>,  $\lambda_{\text{max}} = 672$  nm,  $\epsilon_{\text{max}} = 9300$  cm<sup>-1</sup> M<sup>-1</sup>)<sup>4,6</sup> as oxidants.

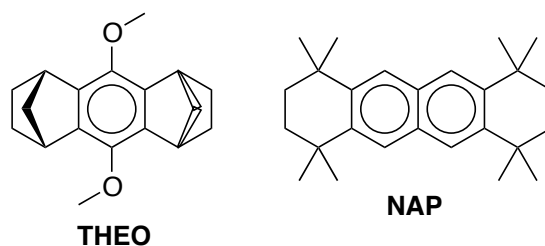


**Figure S2.** Chemical structures and names of the aromatic oxidants used in redox titrations.

Each redox titration experiment was carried out by an incremental addition of sub-stoichiometric amounts of neutral electron donor (**D**) to the solution of an oxidant cation radical (**Ox**<sup>+</sup>). The 1-*e*<sup>-</sup> oxidation of **D** to **D**<sup>+</sup> and reduction of **Ox**<sup>+</sup> to **Ox** can be described by an equilibrium shown in eq. 1.



Numerical deconvolution<sup>7,8</sup> of the UV-VIS absorption spectrum at each increment produced the individual spectra of **D**<sup>+</sup> and **Ox**<sup>+</sup> (Figures S3-S5).

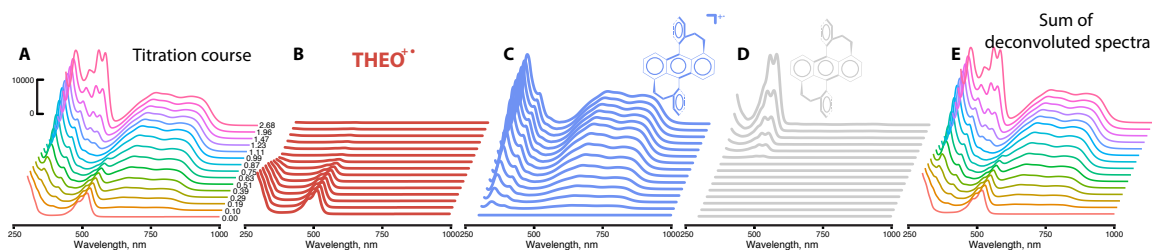


**Figure S3.** A: Spectral changes observed upon the reduction of 0.049 mM  $\text{THEO}^{++}$  (3 mL) by incremental addition (4  $\mu\text{L}$ ) of 3.6 mM solution of  ${}^{\text{S}}\text{ANT}^0$  in  $\text{CH}_2\text{Cl}_2$ . B, C, D: Showing the component spectra of  $\text{THEO}^{++}$  (burgundy),  ${}^{\text{S}}\text{ANT}^{++}$  (blue), and  ${}^{\text{S}}\text{ANT}$  (grey), obtained from the deconvolution of spectrum at each titration point from figure A. E: Sum of the individual spectra of  $\text{THEO}^{++}$ ,  ${}^{\text{S}}\text{ANT}^{++}$  and  ${}^{\text{S}}\text{ANT}^0$ .

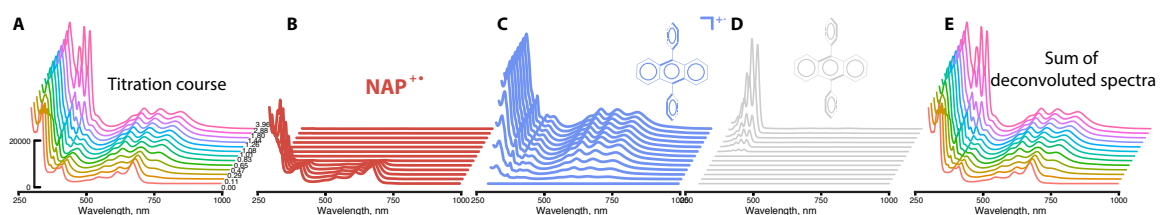


**Figure S4.** Spectral changes observed upon the reduction of 0.056 mM  $\text{NAP}^{++}$  (3 mL) by incremental addition (10  $\mu\text{L}$ ) of 3.0 mM solution of 9,10-diphenyl anthracene ( $\text{DPA}$ ) in  $\text{CH}_2\text{Cl}_2$ . B, C, D: Showing the component spectra of  $\text{NAP}^{++}$  (burgundy),  $\text{DPA}^{++}$  (blue), and  $\text{DPA}$  (grey), obtained from the deconvolution of spectrum at each titration point from figure A. E: Sum of the individual spectra of  $\text{NAP}^{++}$ ,  $\text{DPA}^{++}$  and  $\text{DPA}$ .

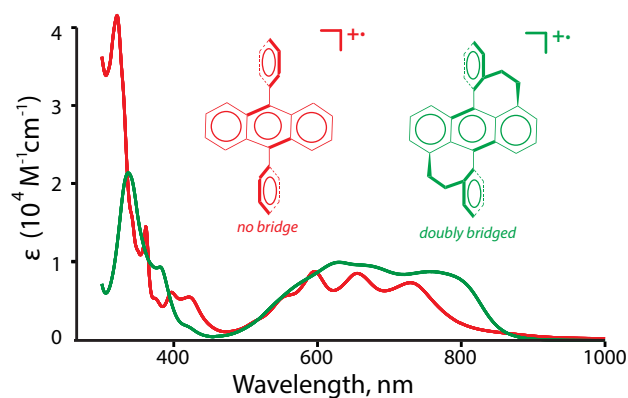
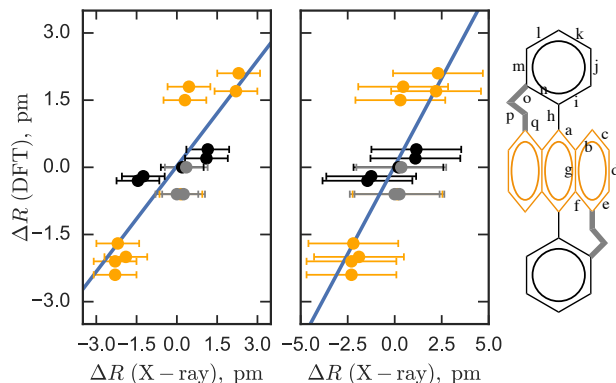


**Figure S5.** Comparison of the absorption spectra of  $\text{DPA}^{++}$  and  ${}^{\text{S}}\text{ANT}^{++}$ .

### S3. X-Ray Crystallography

**Preparation of [ $^{\delta}\text{ANT}^{++}\text{SbCl}_6^-$ ] single crystals using  $\text{NO}^+\text{SbCl}_6^-$ .** A Schlenk tube fitted with a Schlenk adaptor was charged with nitrosonium hexachloroantimonate (92 mg, 0.25 mmol) and anhydrous dichloromethane (20 mL) under an argon atmosphere. Solid  $^{\delta}\text{ANT}$  (96 mg, 0.25 mmol) was added under an argon atmosphere at  $\sim 0$  °C. The solution immediately took on a dark-red coloration, which was stirred (while slowly bubbling argon through the solution to entrain gaseous NO) for 20-30 min to yield a dark-colored solution of cation radical [ $\text{QP}^{++}\text{SbCl}_6^-$ ], vide infra. The solution was carefully layered with dry toluene (30 mL) and placed in a refrigerator ( $-10$  °C) which after 2 days, produced a well-formed crop of single crystals of the [ $^{\delta}\text{ANT}^{++}\text{SbCl}_6^-$ ] suitable for X-ray structure analysis.

**Table S1.** Oxidation-induced C-C bond length changes of  $^{\delta}\text{ANT}$  obtained using X-ray crystallography. Correlation plots between experimental and calculate changes is shown below with error bars corresponding to the standard deviation ( $\sigma = 0.008$  Å, left) and  $3\sigma$  (right), computed from the precisions of the neutral (0.0016 Å) and cation radical (0.0078 Å) structures.



bond	X-ray ( $^{\delta}\text{ANT}$ )	X-ray ( $^{\delta}\text{ANT}^{++}$ )	DFT ( $^{\delta}\text{ANT}$ )	DFT ( $^{\delta}\text{ANT}^{++}$ )	$\Delta$ (DFT), pm	$\Delta$ (X-ray), pm
a	1.4045	1.416	1.401	1.405	0.4	1.15
b	1.3875	1.375	1.387	1.385	-0.2	-1.25
c	1.387	1.389	1.39	1.39	0.0	0.2
d	1.386	1.397	1.388	1.39	0.2	1.1
e	1.3965	1.382	1.393	1.39	-0.3	-1.45
f	1.4015	1.394	1.399	1.403	0.4	-0.75
g	1.4965	1.5	1.498	1.498	0.0	0.35
h	1.5325	1.535	1.532	1.526	-0.6	0.25
i	1.514	1.514	1.52	1.514	-0.6	0.0
j	1.453	1.43	1.448	1.424	-2.4	-2.3
k	1.415	1.437	1.414	1.431	1.7	2.2
l	1.497	1.475	1.493	1.476	-1.7	-2.2
m	1.368	1.391	1.369	1.39	2.1	2.3
n	1.408	1.385	1.41	1.389	-2.1	-2.3
o	1.3585	1.363	1.358	1.376	1.8	0.45
p	1.431	1.412	1.429	1.409	-2.0	-1.9
q	1.4455	1.447	1.446	1.44	-0.6	0.15
r	1.425	1.428	1.416	1.431	1.5	0.3

## S4. Density Functional Theory Calculations

### Computational Details

The electronic structure calculations were performed using density functional theory (DFT) as implemented in Gaussian 09 package, revision D.01<sup>9</sup> using B3LYP-40/6-31G(d)+PCM(CH<sub>2</sub>Cl<sub>2</sub>)<sup>10,11</sup> level of theory.<sup>12</sup> Solvent effects were included using the implicit integral equation formalism polarizable continuum model (IEF-PCM)<sup>13-17</sup> with dichloromethane solvent parameters ( $\epsilon = 8.93$ ). In all DFT calculations, ultrafine Lebedev's grid was used with 99 radial shells per atom and 590 angular points in each shell. Tight cutoffs on forces and atomic displacement were used to determine convergence in geometry optimization procedure. Harmonic vibrational frequency calculations were performed for the optimized structures to confirm absence of imaginary frequencies for equilibrium geometries and presence of one imaginary frequency for transition state geometries. For each transition state a reaction path along the intrinsic reaction coordinate (IRC)<sup>18</sup> was calculated. For cation radicals, wavefunction stability tests<sup>19</sup> were performed to ensure absence of solutions with lower energy. The values of  $\langle S^2 \rangle$  operator after spin annihilation were confirmed to be close to the expectation value of 0.75.

## Isomerization Pathways

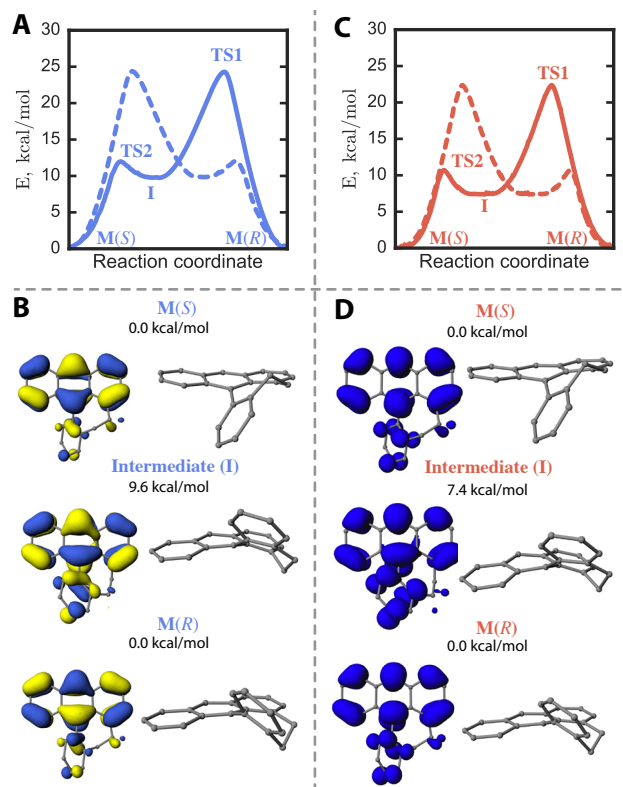


**Figure S6.** IRC (Intrinsic reaction coordinate) pathway of the  $M(R) \rightleftharpoons M(S)$  racemization, the structures, isovalue plots of HOMOs (or spin-density) and Gibbs free energies (in kcal/mol) of transition states (**TS1**, **TS2**) and intermediates (**I**) along the pathway for both neutral (left) and cation radical (right).

**Table S2.** Thermodynamic data for IRC pathway showed in Figure S8 for neutral **M**.

	<b>M(S)</b>	<b>TS1</b>	<b>I</b>	<b>TS2</b>	<b>M(R)</b>
$\Delta E_{\text{elec}}$ , kcal/mol	0.0	23.9	9.6	11.8	0.0
$\Delta G$ , kcal/mol	0.0	24.5	9.4	12.0	0.0
$\Delta H$ , kcal/mol	0.0	23.4	9.5	11.2	0.0
$\Delta S$ , cal/mol/K	0.0	-3.6	0.3	-2.6	0.0

**Table S3.** Thermodynamic data for IRC pathway showed in Figure S8 for  $M^{\bullet+}$ .

	<b>M(S)</b>	<b>TS1</b>	<b>I</b>	<b>TS2</b>	<b>M(R)</b>
$\Delta E_{\text{elec}}$ , kcal/mol	0.0	22.4	7.4	10.7	0.0
$\Delta G$ , kcal/mol	0.0	22.8	7.3	11.0	0.0
$\Delta H$ , kcal/mol	0.0	21.8	7.3	10.2	0.0
$\Delta S$ , cal/mol/K	0.0	-3.4	0.2	-2.8	0.0

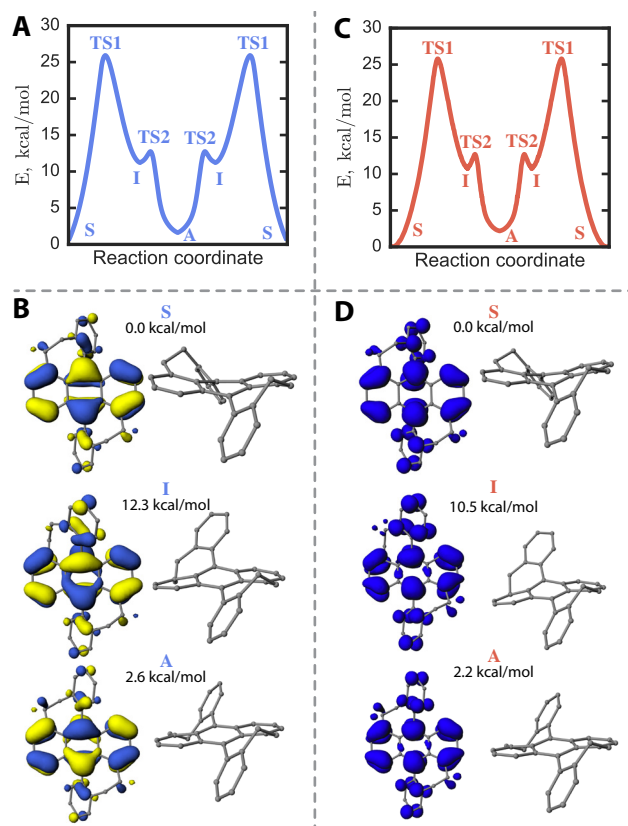


**Figure S7.** IRC (Intrinsic reaction coordinate) pathway of the  ${}^S\text{ANT}(R,R) \rightleftharpoons {}^S\text{ANT}(S,S)$  racemization, the structures, isovalue plots of HOMOs (or spin-density) and Gibbs free energies (in kcal/mol) of transition states (TS1, TS2) and intermediates (I) along the pathway for both neutral (left) and cation radical (right).

**Table S4.** Thermodynamic data for IRC pathway showed in Figure S9 for neutral  ${}^S\text{ANT}$ .

	Syn	TS1	I	TS2	Anti
$\Delta E_{\text{elec}}$ , kcal/mol	0.0	26.7	12.3	13.8	2.6
$\Delta G$ , kcal/mol	0.0	27.6	12.3	14.3	2.8
$\Delta H$ , kcal/mol	0.0	26.1	12.2	13.2	2.6
$\Delta S$ , cal/mol/K	0.0	-4.8	-0.4	-3.6	-0.4

**Table S5.** Thermodynamic data for IRC pathway showed in Figure S9 for  ${}^S\text{ANT}^{\bullet+}$ .

	Syn	TS1	I	TS2	Anti
$\Delta E_{\text{elec}}$ , kcal/mol	0.0	25.6	10.5	12.8	2.2
$\Delta G$ , kcal/mol	0.0	26.4	10.4	13.4	2.4
$\Delta H$ , kcal/mol	0.0	24.9	10.4	12.3	2.2
$\Delta S$ , cal/mol/K	0.0	-5.0	-0.3	-3.8	-0.8

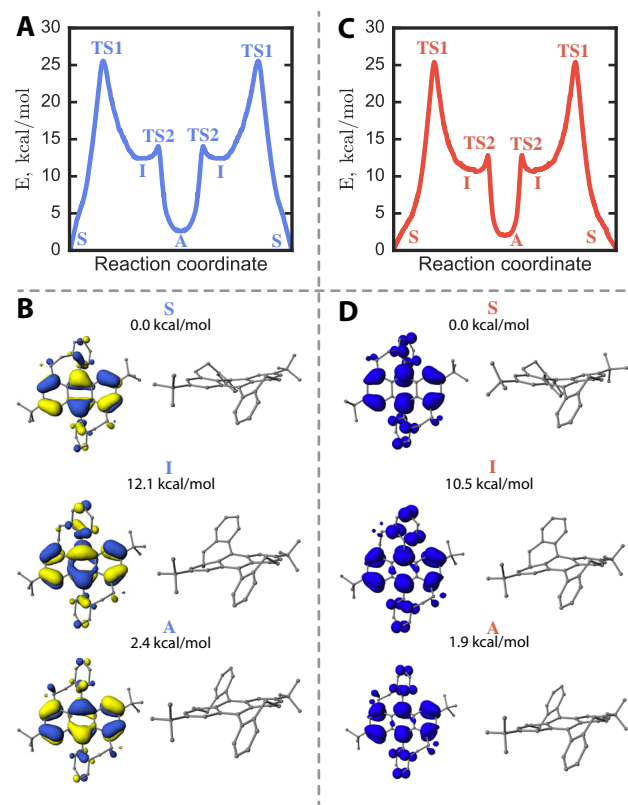


**Figure S8.** IRC (Intrinsic reaction coordinate) pathway of the  $A(R,R) \rightleftharpoons A(S,S)$  racemization, the structures, isovalue plots of HOMOs (or spin-density) and Gibbs free energies (in kcal/mol) of transition states (**TS1**, **TS2**) and intermediates (**I**) along the pathway for both neutral (left) and cation radical (right).

**Table S6.** Thermodynamic data for IRC pathway showed in Figure S10 for neutral **A**.

	<b>Syn</b>	<b>TS1</b>	<b>I</b>	<b>TS2</b>	<b>Anti</b>
$\Delta E_{\text{elec}}$ , kcal/mol	0.0	26.3	12.1	13.7	2.4
$\Delta G$ , kcal/mol	0.0	26.9	12.1	14.2	2.5
$\Delta H$ , kcal/mol	0.0	25.7	12	13.1	2.4
$\Delta S$ , cal/mol/K	0.0	-3.9	-0.2	-3.6	-0.4

**Table S7.** Thermodynamic data for IRC pathway showed in Figure S10 for **A<sup>+</sup>**

	<b>Syn</b>	<b>TS1</b>	<b>I</b>	<b>TS2</b>	<b>Anti</b>
$\Delta E_{\text{elec}}$ , kcal/mol	0.0	25.3	10.5	12.8	1.9
$\Delta G$ , kcal/mol	0.0	26.0	10.5	13.7	2.1
$\Delta H$ , kcal/mol	0.0	24.6	10.5	12.3	1.9
$\Delta S$ , cal/mol/K	0.0	-4.9	0.0	-4.6	-0.6

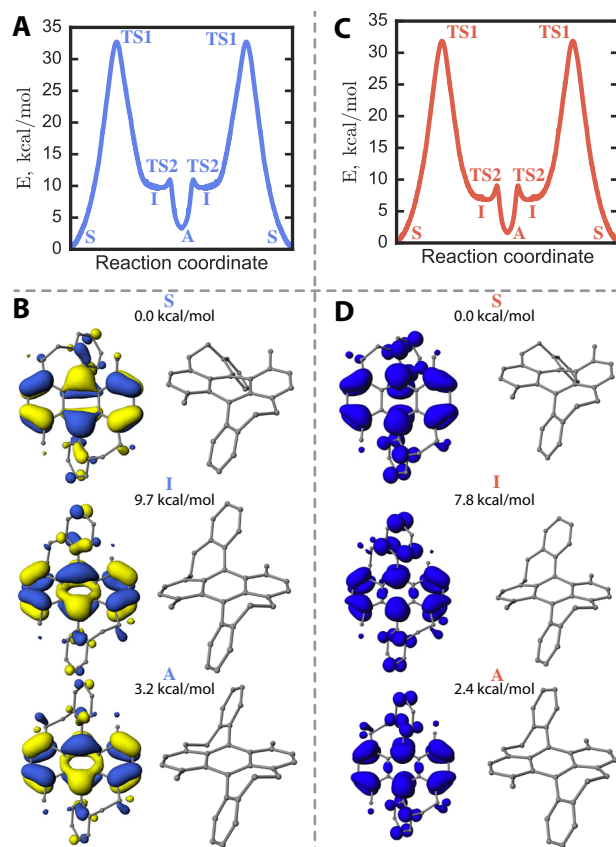


**Figure S9.** IRC (Intrinsic reaction coordinate) pathway of the  $\mathbf{B}(R,R) \rightleftharpoons \mathbf{B}(S,S)$  racemization, the structures, isovalue plots of HOMOs (or spin-density) and Gibbs free energies (in kcal/mol) of transition states (**TS1**, **TS2**) and intermediates (**I**) along the pathway for both neutral (left) and cation radical (right).

**Table S8.** Thermodynamic data for IRC pathway showed in Figure S11 for neutral **B**

	Syn	TS1	I	TS2	Anti
$\Delta E_{\text{elec}}$ , kcal/mol	0.0	33.5	9.7	10.9	3.2
$\Delta G$ , kcal/mol	0.0	34.3	9.4	11.3	3.1
$\Delta H$ , kcal/mol	0.0	32.6	9.5	10.3	3.1
$\Delta S$ , cal/mol/K	0.0	-5.4	0.2	-3.3	0.1

**Table S9.** Thermodynamic data for IRC pathway showed in Figure S11 for  $\mathbf{B}^{+\bullet}$

	Syn	TS1	I	TS2	Anti
$\Delta E_{\text{elec}}$ , kcal/mol	0.0	32.9	7.8	10.1	2.4
$\Delta G$ , kcal/mol	0.0	34.0	7.8	10.5	2.4
$\Delta H$ , kcal/mol	0.0	32.0	7.6	9.4	2.2
$\Delta S$ , cal/mol/K	0.0	-6.8	-0.9	-3.8	-0.8

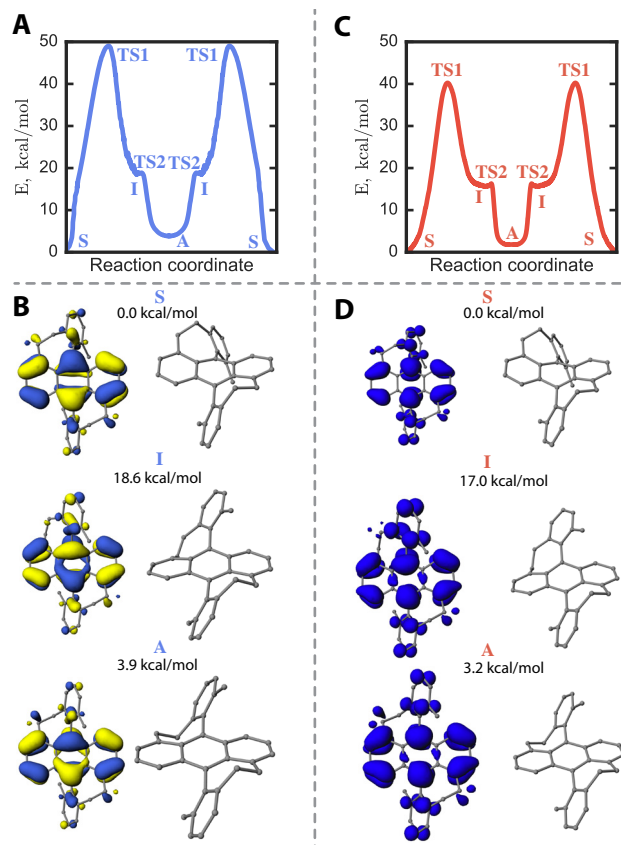


**Figure S10.** IRC (Intrinsic reaction coordinate) pathway of the  $C(R,R) \rightleftharpoons C(S,S)$  racemization, the structures, isovalue plots of HOMOs (or spin-density) and Gibbs free energies (in kcal/mol) of transition states (TS1, TS2) and intermediates (I) along the pathway for both neutral (left) and cation radical (right).

**Table S10.** Thermodynamic data for IRC pathway showed in Figure S12 for neutral C

	Syn	TS1	I	TS2	Anti
$\Delta E_{\text{elec}}$ , kcal/mol	0.0	50.3	18.6	18.7	3.9
$\Delta G$ , kcal/mol	0.0	51.2	18.6	19.4	4.1
$\Delta H$ , kcal/mol	0.0	49.3	18.5	18.1	3.9
$\Delta S$ , cal/mol/K	0.0	-6.2	-0.4	-4.3	-0.6

**Table S11.** Thermodynamic data for IRC pathway showed in Figure S12 for  $C^{+\bullet}$

	Syn	TS1	I	TS2	Anti
$\Delta E_{\text{elec}}$ , kcal/mol	0.0	41.7	17.0	17.7	3.2
$\Delta G$ , kcal/mol	0.0	42.2	16.6	18.3	3.0
$\Delta H$ , kcal/mol	0.0	40.5	16.8	17.1	3.1
$\Delta S$ , cal/mol/K	0.0	-5.8	0.5	-3.9	0.3

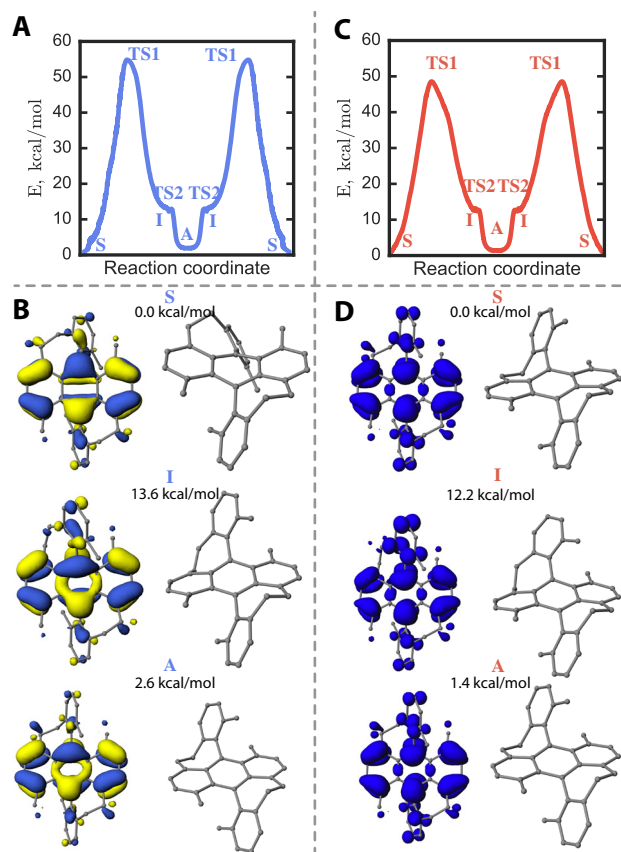


**Figure S11.** IRC (Intrinsic reaction coordinate) pathway of the  $D(R,R) \rightleftharpoons D(S,S)$  racemization, the structures, isovalue plots of HOMOs (or spin-density) and Gibbs free energies (in kcal/mol) of transition states (TS1, TS2) and intermediates (I) along the pathway for both neutral (left) and cation radical (right).

**Table S12.** Thermodynamic data for IRC pathway showed in Figure S13 for neutral **D**

	Syn	TS1	I	TS2	Anti
$\Delta E_{\text{elec}}$ , kcal/mol	0.0	56.0	13.6	13.6	2.6
$\Delta G$ , kcal/mol	0.0	56.7	13.1	14.1	2.6
$\Delta H$ , kcal/mol	0.0	54.7	13.4	12.8	2.5
$\Delta S$ , cal/mol/K	0.0	-6.7	1	-4.4	-0.5

**Table S13.** Thermodynamic data for IRC pathway showed in Figure S13 for  $D^{\bullet+}$

	Syn	TS1	I	TS2	Anti
$\Delta E_{\text{elec}}$ , kcal/mol	0.0	50.9	12.2	12.7	1.4
$\Delta G$ , kcal/mol	0.0	50.9	11.9	12.6	1.0
$\Delta H$ , kcal/mol	0.0	49.4	11.9	11.9	1.1
$\Delta S$ , cal/mol/K	0.0	-5.1	0.0	-2.5	0.4

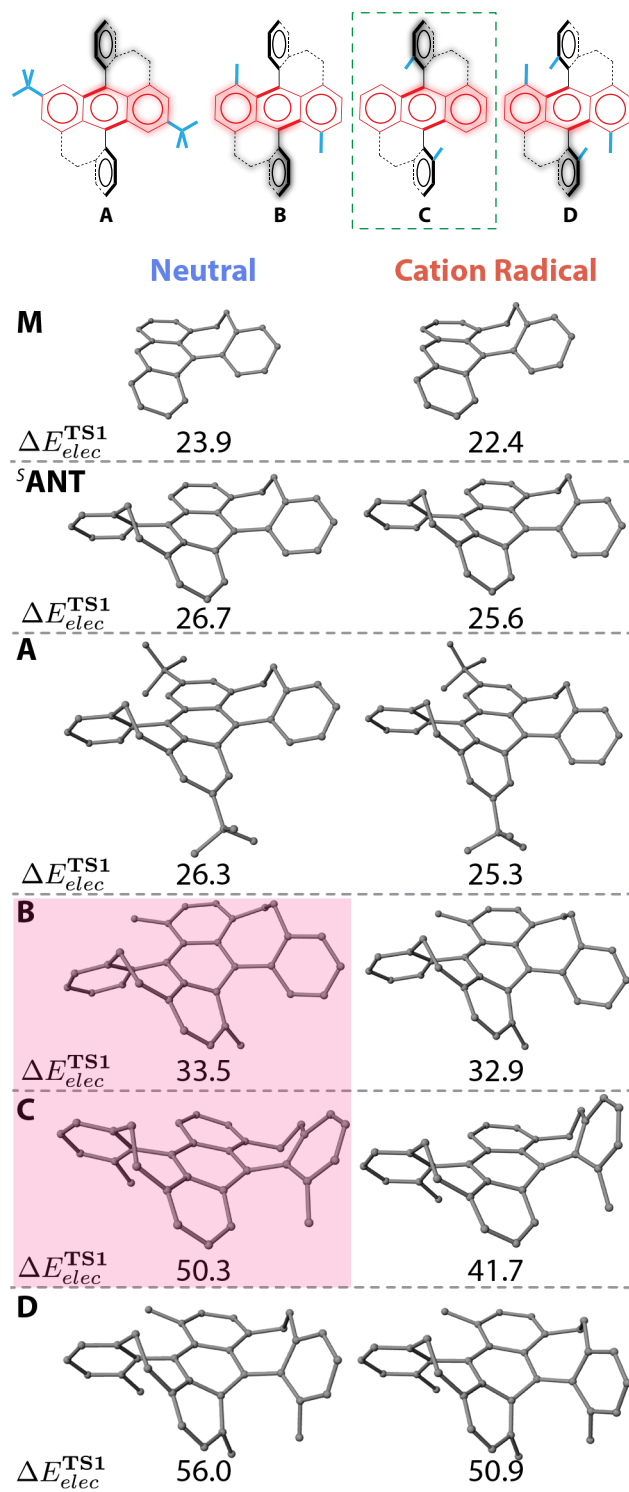


**Figure S12.** Structures of the transition states (TS1) of various <sup>S</sup>ANT derivatives shown in Figure 7 in the manuscript in neutral and cation radical states

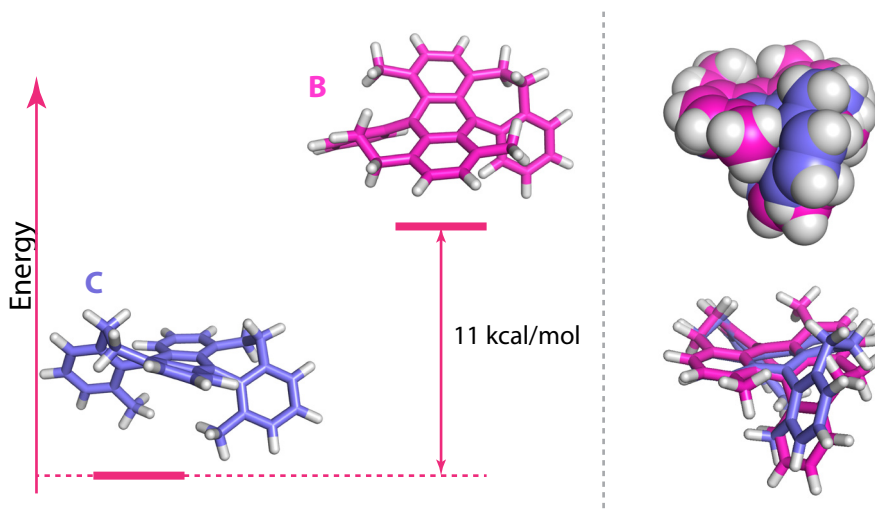


**Figure S13.** Showing that the energy difference between structures **B** and **C** arises from steric crowding between the methyl substituents on anthracene core and phenyl groups

## S5. Kinetic Modeling

The Eyring equation defines the rates  $k$  of a chemical reaction as follows:

$$k = \frac{k_B T}{h} e^{-\frac{\Delta G^\ddagger}{RT}} \text{ (eq. 1)}$$

where  $\Delta G^\ddagger = \Delta H^\ddagger - T\Delta S^\ddagger$  is the Gibbs free energy of activation,  $\Delta H^\ddagger$  is enthalpy of activation,  $\Delta S^\ddagger$  is entropy of activation,  $k_B$  is Boltzmann's constant and  $h$  is Planck's constant. Using the available rate constants of  $^S\text{ANT}$  racemization at different temperatures (Table S14) and the linearized Eyring equation (eq. 2), Gibbs free energy, enthalpy and entropy of activation at room temperature (298.15 K) were determined (Figure S16, Table S15)

$$\ln \frac{k}{T} = -\frac{\Delta H^\ddagger}{R} \frac{1}{T} + \ln \frac{k_B}{h} + \frac{\Delta S^\ddagger}{R} \text{ (eq. 2)}$$

The half-life of the racemization can be expressed using the first-order kinetic equation:

$$t_{1/2} = \frac{\ln 2}{k} \text{ (eq. 3)}$$

Using the experimental Gibbs free energy of activation (Table S15), the half-life of  $^S\text{ANT}$  racemization is 1.1 hours.

**Table S14.** Rate constants of the racemization process in <sup>S</sup>ANT from ref. 1.

$k \times 10^5, s^{-1}$	T, °C
7.85	19.3
56	34.5
298	50.0

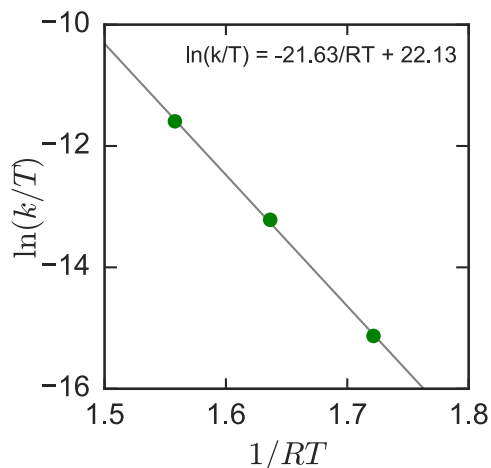
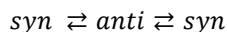


**Figure S14.** Plot of racemization rate constants of <sup>S</sup>ANT against temperature using the linear form of the Eyring equation using data from ref. 1. Green symbols and grey line denote experimental points and a trendline, respectively.

**Table S15.** Thermodynamic data on the racemization in <sup>S</sup>ANT obtained from Eyring equation and kinetic data in Table S14 using kinetic data from ref. 1.

$\Delta G^\ddagger$ , kcal/mol	22.6
$\Delta H^\ddagger$ , kcal/mol	21.6
$\Delta S^\ddagger$ , cal/mol/K	-3.2

According to the results from DFT calculations (Figures S6-S11), racemization mechanism between *syn* enantiomers in all studied compounds (**M**, <sup>S</sup>ANT, **A**, **B**, **C** and **D** in both neutral and cation radical states) involves achiral *anti* conformation that is 1-2 kcal/mol higher than *syn*. Note that the presence of the high-energy intermediate between *syn* and *anti* conformations does not significantly impact the overall kinetics of the interconversion. Thus, the interconversion between *syn* and *anti* conformations can be described by the following equilibrium equation:



Solving the following system of differential equations the time evolution of concentrations of each species can be simulated:

$$\frac{d[\mathbf{S1}]}{dt} = -k_{sa}[\mathbf{S1}] + k_{as}[\mathbf{A}]$$

$$\frac{d[\mathbf{A}]}{dt} = k_{sa}[\mathbf{S1}] - 2k_{as}[\mathbf{A}] + k_{sa}[\mathbf{S2}]$$

$$\frac{d[\mathbf{S2}]}{dt} = -k_{sa}[\mathbf{S2}] + k_{as}[\mathbf{A}]$$

where rate constants  $k_{sa}$  and  $k_{as}$  between syn and anti conformations can be determined from the Eyring equation at room temperature.

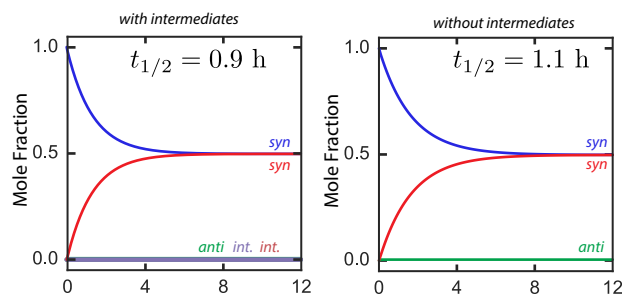


**Figure S15.** Effect of the intermediates on the kinetics of the racemization process in  $^S\text{ANT}$ .

**Table S16.** Computed activation energies of racemization ( $\Delta G^\ddagger$ , kcal/mol) and racemization half-lives ( $t_{1/2}$ ) of  $^S\text{ANT}$  derivatives scaled to reproduce experimentally observed activation energy of  $^S\text{ANT}$  (ref. 1).

Compound	$\Delta G^\ddagger$ , kcal/mol	$t_{1/2}$
$^S\text{ANT}$	22.6	1.1 h
<b>M</b>	19.5	22 s
<b>A</b>	21.9	0.4 h
<b>B</b>	29.3	10.6 y
<b>C</b>	46.2	$2.6 \times 10^{13}$ y
<b>D</b>	51.7	$2.8 \times 10^{21}$ y

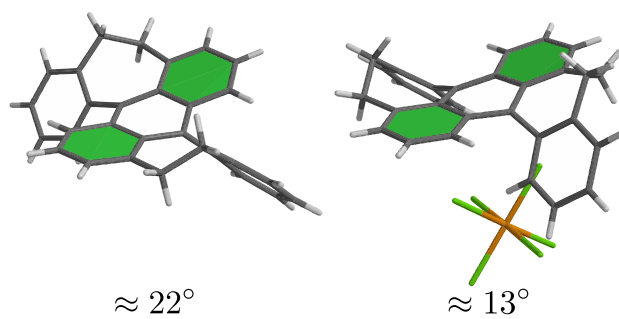


**Figure S16.** Interplanar angles between phenylene moieties (shaded green) of the anthracene cores in  ${}^S\text{ANT}$  and  ${}^S\text{ANT}^+$  crystal structures.

**Table S17.** Imaginary frequencies ( $\text{cm}^{-1}$ ) of the transition states of various **ANT** derivatives

	Neutral		Cation radical	
	TS1	TS2	TS1	TS2
<b>M</b>	-112.5	-143.9	-133.5	-155
<b>ANT</b>	-75.3	-127.4	-89.7	-141.4
<b>A</b>	-70.3	-128.5	-91.2	-141.7
<b>B</b>	-55.1	-113.3	-54.8	-129
<b>C</b>	-55	-82.5	-45.3	-116.7
<b>D</b>	-32.4	-40.3	-49.1	-114.4

## S6. References

- (1) I. Agranat, M. R. Suissa, S. Cohen, R. Isaksson, J. Sandström, J. Dale, and D. Grace, *Chem. Comm.* 1987, 381.
- (2) I. Agranat, S. Cohen, R. Isaksson, J. Sandstroem, and M. R. Suissa, *J. Org. Chem.* 1990, **55**, 4943.
- (3) R. Rathore, C. L. Burns, and M. I. Deselnicu, *Org. Synth.* 2005, 1.
- (4) R. Rathore and J. K. Kochi, *Acta. Chem. Scand.* 1998, **52**, 114.
- (5) R. Rathore, C. L. Burns, and M. I. Deselnicu, *Org. Lett.* 2001, **3**, 2887.
- (6) R. Rathore and J. K. Kochi, *Acta. Chem. Scand.* 1998, **52**, 114.
- (7) M. R. Talipov, A. Boddeda, M. M. Hossain, and R. Rathore, *J. Phys. Org. Chem.* 2015, **29**, 227.
- (8) M. R. Talipov, M. M. Hossain, A. Boddeda, K. Thakur, and R. Rathore, *Org. Biomol. Chem.* 2016, **14**, 2961.
- (9) Frisch, M. J.; Trucks, G. W.; Schlegel, H. B.; Scuseria, G. E.; Robb, M. A.; Cheeseman, J. R.; Scalmani, G.; Barone, V.; Mennucci, B.; Petersson, G. A.; Nakatsuji, H.; Caricato, M.; Li, X.; Hratchian, H. P.; Izmaylov, A. F.; Bloino, J.; Zheng, G.; Sonnenberg, J. L.; Hada, M.; Ehara, M.; Toyota, K.; Fukuda, R.; Hasegawa, J.; Ishida, M.; Nakajima, T.; Honda, Y.; Kitao, O.; Nakai, H.; Vreven, T.; Montgomery, J. A. A.; Peralta, J. E.; Ogliaro, F.; Bearpark, M.; Heyd, J. J.; Brothers, E.; Kudin, K. N.; Staroverov, V. N.; Kobayashi, R.; Normand, J.; Raghavachari, K.; Rendell, A.; Burant, J. C.; Iyengar, S. S.; Tomasi, J.; Cossi, M.; Rega, N.; Millam, J. M.; Klene, M.; Knox, J. E.; Cross, J. B.; Bakken, V.; Adamo, C.; Jaramillo, J.; Gomperts, R.; Stratmann, R. E.; Yazyev, O.; Austin, A. J.; Cammi, R.; Pomelli, C.; Ochterski, J. W.; Martin, R. L.; Morokuma, K.; Zakrzewski, V. G.; Voth, G. A.; Salvador, P.; Dannenberg, J. J.; Dapprich, S.; Daniels, A. D.; Farkas; Foresman, J. B.; Ortiz, J. V.; Cioslowski, J.; Fox, D. J. Gaussian, Inc., Wallingford CT, 2009.
- (10) W. J. Hehre, R. Ditchfield, and J. A. Pople, *J. Chem. Phys.* 1972, **56**, 2257.
- (11) C. Adamo and V. Barone, *Chem. Phys. Lett.* 1997, **274**, 242.
- (12) M. R. Talipov, A. Boddeda, Q. K. Timerghazin, and R. Rathore, *J. Phys. Chem. C.* 2014, **118**, 21400.
- (13) J. Tomasi, B. Mennucci, and R. Cammi, *Chem. Rev.* 2005, **105**, 2999.
- (14) S. Miertu, E. Scrocco, and J. Tomasi, *Chem. Phys.* 1981, **55**, 117.
- (15) M. Cossi, V. Barone, B. Mennucci, and J. Tomasi, *Chem. Phys. Lett.* 1998, **286**, 253.
- (16) E. Cancès, B. Mennucci, and J. Tomasi, *J. Chem. Phys.* 1997, **107**, 3032.
- (17) R. F. Ribeiro, A. V. Marenich, C. J. Cramer, and D. G. Truhlar, *J. Phys. Chem. B.* 2011, **115**, 14556.
- (18) K. Fukui, *Acc. Chem. Res.* 1981, **14**, 363.
- (19) R. Bauernschmitt and R. Ahlrichs, *J. Chem. Phys.* 1996, **104**, 9047.